arXiv:2507.03977v1 [eess.SP] 5 Jul 2025

MMOC: Self-Supervised EEG Emotion Recognition Framework with Multi-Model Online Collaboration

Hanqi Wang, Yang Liu, Peng Ye, Liang Song

[a]*Fudan Univeristy, Shanghai,*

Abstract

Electroencephalography (EEG) emotion recognition plays a crucial role in human-computer interaction, particularly in healthcare and neuroscience. While supervised learning has been widely used, its reliance on manual annotations introduces high costs and potential bias. Self-supervised learning (SSL) offers a promising alternative by generating labels through pretext tasks. However, high inter-subject variability in EEG signals leads to significant data drift, limiting self-supervised models' generalization across unseen subjects. Traditional domain adaptation (DA) methods require access to target-domain data during training—an impractical requirement in many real-world applications. Although domain generalization (DG) avoids this constraint, it often falls short in handling complex data drift due to limited coverage of possible target distributions. To tackle these challenges, we propose MMOC, a self-supervised framework with multi-model online collaboration (MMOC), to achieve online adaptation to unseen data. MMOC trains multiple base models using diverse strategies rooted in reconstruction and contrastive learning, enabling each model to develop distinct generalization capabilities. During inference, MMOC dynamically activates the most suitable model for each test sample via a loss-based routing mechanism that evaluates both contrastive and reconstruction losses. This dual consideration allows for a comprehensive measurement of data drift at both structural and semantic levels. Experimental results on the SEED and Dreamer datasets show that MMOC achieves state-of-the-art performance: 85.39% ± 5.41 on SEED, and 68.77% ± 6.13 / 69.37% ± 7.11 on Dreamer arousal and valence dimensions, respectively. MMOC effectively mitigates inter-subject data drift, offering a practical solution for real-world EEG emotion recognition.

Keywords: Electroencephalogram (EEG), self-supervised learning, emotion

recognition, multi-model online collaboration

1. Introduction

Emotion recognition through brain-computer interfaces (BCIs) has become increasingly important in advancing human-computer interaction, particularly in domains such as medicine and neuroscience. Electroencephalography (EEG) is widely regarded as a favorable modality for emotion assessment due to its non-invasive nature, objectivity, and high temporal resolution [1, 2]. The integration of deep learning techniques into EEG-based emotion recognition has led to substantial progress, transforming how emotional states are inferred from neural signals. Historically, most approaches have relied on supervised learning paradigms that require access to large-scale labeled datasets for training. However, acquiring such annotated data presents notable challenges, as manual labeling is labor-intensive and time-consuming [1, 2]. Moreover, label accuracy often depends on subjective self-reports or expert interpretation, which can introduce inconsistencies and bias, ultimately affecting model reliability [2].

To address this limitation, recent studies have increasingly explored self-supervised learning strategies aimed at extracting robust and generalizable representations from unlabeled EEG data for downstream emotion recognition tasks [3, 4, 5, 6]. These methods typically leverage pretext tasks that automatically generate supervisory signals, thereby reducing reliance on manually labeled annotations. Recent advancements have highlighted the promise of self-supervised learning in the context of EEG-based emotion recognition. Nevertheless, the high inter-subject variability introduces a significant challenge in the form of EEG data drift [1, 2]. In the inference phase, models frequently struggle to generalize effectively to data from unseen subjects. This limitation severely constrains the practical applicability of self-supervised models in real-world applications. Current research primarily focuses on exploring domain generalization and domain adaptation techniques to address this inter-subject data drift problem. Domain adaptation (DA) techniques mitigate this problem through the alignment of the target domain with the source domain. However, models based on domain adaptation techniques cannot be directly applied to unseen data without a calibration process. This process usually requires access to the target domain, which is often unavailable in practical applications. This limitation

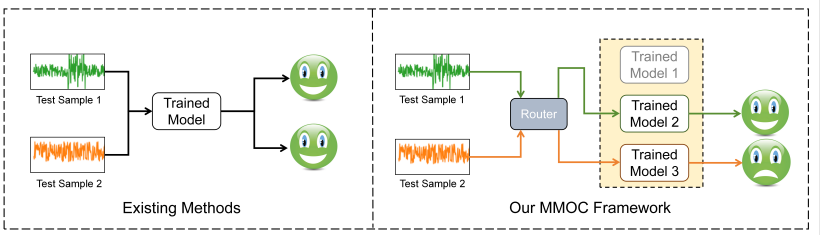

Figure 1: The demonstration of the existing methods and the proposed one. Most existing state-of-the-art methods (as illustrated in the left panel) depend on a single model for inference, which inherently limits their ability to generalize across diverse data distributions. In contrast, our framework (right panel) leverages an ensemble of multiple models and employs a dynamic routing mechanism that selects the most appropriate model based on the characteristics of each input sample. This design significantly improves the model's adaptability and coverage over varying test data distributions.

hinders their practical application in real-world scenarios. Domain generalization (DG) techniques aim to capture the shared characteristics in the source domain, thereby achieving generalizability on the unseen target domain. Thus, DG methods eliminate the necessity for a calibration process and bypass the requirement for access to the target domain. However, the effectiveness of DG relies on the assumption that the source domain can cover part of the target domain's distribution. When confronted with complex data drift, DG models based on source domains may fail to cover the target domain's distribution. This results in a decline in model performance on unseen data.

This observation motivates us to explore a novel self-supervised framework to address the issue of data drift. Even when capable of capturing shared characteristics across subjects, a single DG model remains insufficiently equipped to address the data drift issue when confronted with a complex target domain. Therefore, a more promising approach is to implement online collaboration among multiple models, each possessing differentiated generalization capabilities. During inference, when encountering previously unseen data, the framework activates the appropriate model based on intrinsic characteristics of the input sample. This method enhances the framework's real-time coverage of potential target domains via online collaboration among multiple models, while simultaneously eliminating the need for a calibration process and access to target domain data.

In this work, we introduce a novel self-supervised framework for EEG-

based emotion recognition with multi-model online collaboration (MMOC). The advancement of this framework lies in the collaboration of multiple models, rather than relying on a single model. By employing diverse training strategies, MMOC prepares multiple differentiated models as the candidate pool. When faced with new data in the inference phase, the framework utilizes a dynamic routing mechanism to activate the most suitable model within the candidate pool, adapting to the target domain's data distribution. A primary challenge of this framework lies in defining a real-time unsupervised metric to guide the routing process. Existing studies have shown that the error of reconstruction models can reflect a model's adaptability to new data [7, 8]. However, reconstruction loss primarily focuses on the ability to restore data at the structural level while neglecting potential drifts at the semantic level. Relying solely on reconstruction loss may lead to situations where out-of-distribution (OOD) samples are also well reconstructed—particularly when these OOD samples exhibit structural similarities to the training data. To address this limitation, our base model incorporates both reconstruction and contrastive tasks. The contrastive loss is also employed to measure data drift at the complex semantic level. During the inference phase, the routing policy activates the appropriate model by jointly considering both the reconstruction loss and the contrastive loss. Through routing and the activation of the optimal model, our framework achieves online adaptation without requiring access to the target domain or calibration. The experiments were conducted on the SEED and Dreamer datasets. Our method achieved an accuracy of $85.39\% \pm 5.41$ on the SEED dataset, and accuracies of $68.77\% \pm 6.13$ and $69.37\% \pm 7.11$ on the Arousal and Valence dimensions of the Dreamer dataset, respectively. The contributions of our work can be summarized as follows:

1. This work proposes a multi-model online online collaboration framework for self-supervised EEG emotion recognition. The framework adaptively selects and activates models according to the intrinsic features of each test sample, enabling effective adaptation to diverse and evolving data distributions.
2. This work introduces a novel routing mechanism that leverages both reconstruction loss and contrastive loss. By jointly considering these two complementary metrics, MMOC captures distribution drifts at both structural level and semantic level, which in turn serves as the dynamic routing evidence.

3. We conducted extensive experiments on two public affective EEG datasets, SEED and Dreamer. Compared to existing state-of-the-art methods, our approach demonstrates superior subject-independent performance, highlighting its effectiveness in addressing data distribution drifts.

2. Related Work

2.1. Subject-Independent EEG Emotion Recognition

The increasing demand for practical EEG-based emotion recognition systems has driven significant interest in subject-independent approaches—those capable of recognizing emotional states across diverse individuals. A major obstacle in this domain arises from the high inter-subject variability in EEG signals, which hampers the transfer of learned knowledge from training subjects to unseen test subjects. To mitigate this issue, two primary strategies have been proposed: domain adaptation (DA) and domain generalization (DG).

Domain adaptation aims to reduce the distributional gap between source and target domains by aligning their feature spaces. Zheng et al. [9] demonstrated the effectiveness of classical DA techniques on the SEED dataset. Building upon this, domain-adversarial neural networks (DANNs) were introduced in [10], incorporating a domain classifier to learn features that are invariant across domains. This approach inspired further developments such as the bi-hemisphere domain-adversarial neural network (Bi-DANN) [11] and the regularized graph neural network (RGNN) [12]. Bi-DANN utilizes dual hemisphere classifiers alongside a global classifier to extract subject-invariant emotional representations, while RGNN introduces node-wise adversarial training within a graph-based framework. Despite the improvements offered by DA methods, they typically require access to target domain data during training, limiting their applicability in real-world scenarios where test data may not be available.

In contrast, domain generalization offers a more flexible alternative by aiming to learn subject-invariant representations that generalize across previously unseen individuals without relying on target domain information. For example, Ma et al. [13] extended DANN into a DG framework, proposing a domain residual network (DResNet) that separates domain-shared parameters from domain-specific ones. Nevertheless, current subject-independent methods—regardless of whether they are grounded in DA or DG—primarily adhere to supervised learning frameworks. This dependency constrains their

effectiveness in terms of scalability and real-world deployment, where labeled data may be scarce or impractical to obtain.

2.2. Self-Supervised Representation Learning for EEG Emotion Recognition

Self-supervised learning has achieved impressive results across multiple domains, including computer vision and natural language processing [14, 15, 16, 17, 18, 19]. In recent years, this paradigm has started to gain attention in the context of EEG-based emotion recognition [1, 2], where it offers a promising alternative for extracting informative and transferable feature representations without relying on labeled data.

Several self-supervised pretext tasks have been investigated for EEG signal modeling. For example, transformation-based tasks have been utilized as a form of pretraining in works such as [4, 20], where models are trained to recognize artificially applied transformations on raw EEG signals. Contrastive learning methods have also been adapted to this domain, with studies like [3] introducing a group meiosis strategy to capture shared emotional patterns across subjects. Moreover, reconstruction-oriented tasks have proven effective in generating useful representations for downstream applications, as demonstrated in [21, 22].

Despite these encouraging outcomes, the majority of current approaches still operate under subject-dependent assumptions, which limits their generalization across different individuals. To overcome this limitation, recent studies have explored integrating self-supervised strategies into subject-independent frameworks. One prominent example is CLISA [5], which introduces a contrastive learning framework tailored for cross-subject EEG emotion recognition. By forming positive sample pairs from different individuals exposed to the same emotional stimuli, CLISA achieves improved performance over previous techniques, including those proposed in [13]. Moreover, multi-task self-supervised frameworks have been developed to further enhance inter-subject generalization. The work in [23] combines jigsaw puzzle solving with contrastive objectives to encourage the model to learn more robust and generalized features. Similarly, MSLTE [24] leverages channel masking and frequency masking as auxiliary reconstruction tasks to improve the cross-subject adaptability of learned representations. Collectively, these contributions have pushed forward the development of self-supervised EEG emotion recognition systems. However, existing self-supervised approaches to handling inter-subject variability predominantly depend on either calibrating with test data or extracting invariant features across subjects. Consequently,

these methods continue to operate within the constraints of a single-model framework, limiting their adaptability and generalization capabilities in real-world scenarios involving unseen subjects.

3. Method

The architecture of MMOC is illustrated in the figure. MMOC consists of two stages: training and inference. During the training stage, each base model is trained using a diversified strategy, jointly optimized through both contrastive and reconstruction tasks. Additionally, we assign a classifier to each base model to establish the mapping from learned representations to class labels. In the inference stage, the proposed routing algorithm guides the MMOC to activate the models based on their reconstruction and contrastive outputs.

3.1. Base Model and Classifier Training

Our framework uses reconstruction and contrastive loss as the metric for dynamic routing. Therefore, the base models need to be designed based on a reconstruction and a contrastive task. We adopt a cascaded combination of reconstruction and contrastive tasks. The reconstruction task aims to reconstruct the differential entropy (DE) values across multiple frequency bands from the raw EEG signals, thereby guiding the network to capture structural features. In contrast, the contrastive task aligns the reconstructed outputs with the ground truth in a high-dimensional space, focusing on capturing semantic-level information. The specific architecture of the base model will be elaborated in the following sections 3.3.

Furthermore, a variety of training strategies are implemented to encourage the development of diverse generalization abilities among the multiple models. In addition to the original base model, we construct two other variant models. In the first variant, we employed random masking of the input. We generate a mask $m \in [0,1]^{C\times T}$ for each input $x \in R^{C\times T}$. And then, we obtain the mask sample $x_{mask} = x \odot m$, where $\odot$ represents element-wise multiplication. In the second variant, we added $L2$ regularization to the loss and dropout layer to the model structure. Each base model outputs three components: the latent representation, the reconstructed output, and the

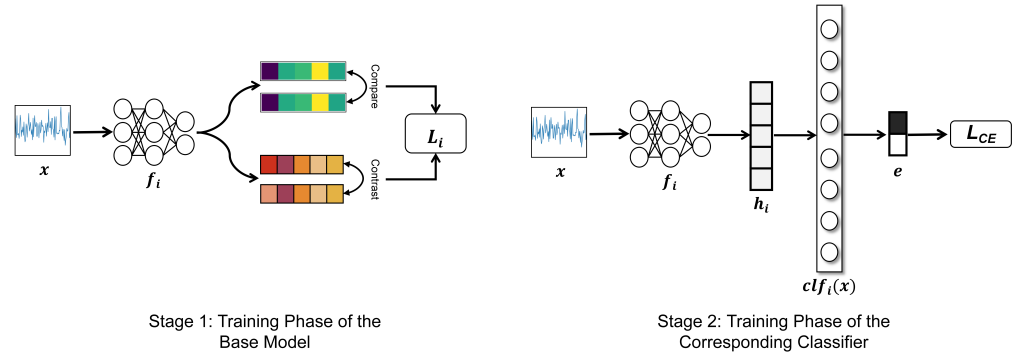

(a) The Training Phase

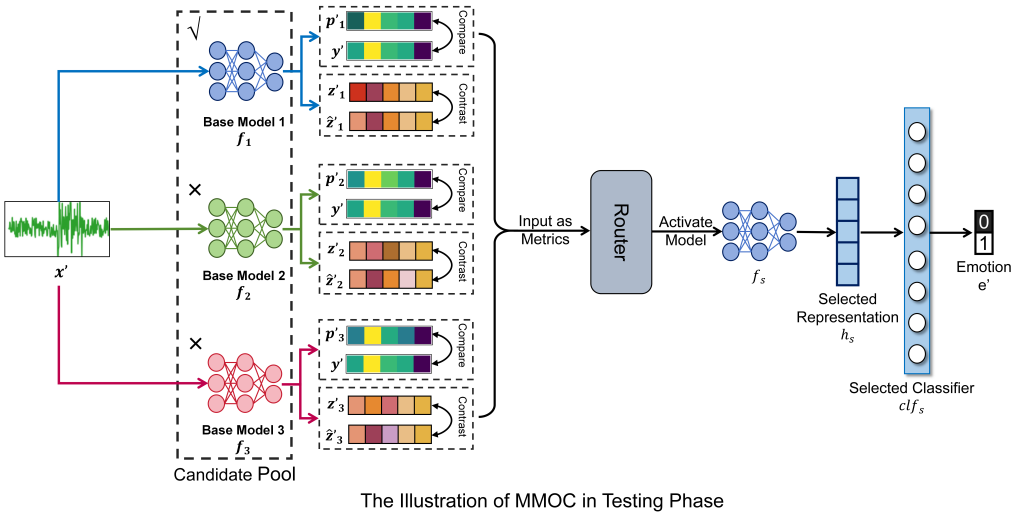

(b) The Inference Phase with MMOC

Figure 2: The demonstration of MMOC framework. In the top figure, we depict the training process of the base models within the MMOC framework. Each base model optimizes its representation learning architecture based on a combination of reconstruction results and contrastive loss. For each base model, a classifier is trained to map the learned representations to predictions. In the bottom figure, we illustrate the workflow of MMOC during prediction. When a test sample enters the framework, multiple base models independently generate reconstruction results and contrastive embeddings. The router then uses them as metric to determine which base model and its corresponding classifier are best suited for the input. This selected model produces the final inference result.

high-dimensional embedding, as follows:

$$\begin{aligned} h_1, p_1, z_1, \hat{z}_1 =& f_1(x), \\ h_2, p_2, z_2, \hat{z}_2 =& f_2(x_{mask}), \\ h_3, p_3, z_3, \hat{z}_3 =& f_3(x). \end{aligned} \tag{1}$$

The f_1, f_2 and f_3 denote the three base models, h_1, h_2 and h_3 denote the learned representations, p_1, p_2 and p_3 denote the reconstructed DE features, z_1, z_2 and z_3 denote the embeddings of reconstructions in the high-dimensional space, and $\hat{z}_1$, $\hat{z}_2$ and $\hat{z}_3$ denote the embeddings of ground truth in the high-dimensional space.

And then, the training objective of the base model is to minimize the combination of reconstruction and contrastive loss. Assume the training set has N samples. Let $P_j = \{p_j^i | i = 1, 2, \ldots, N\}, j \in 1, 2, 3\}$ denote the reconstructions from the j_{th} model, $Z_j = \{z_j^i | i = 1, 2, \ldots, N\}, j \in 1, 2, 3$ denote the embeddings of reconstructions from the j_{th} model, $\hat{Z}_j = \{\hat{z}_j^i | i = 1, 2, \ldots, N\}, j \in 1, 2, 3\}$ denote the embeddings of ground truth from the j_{th} model, and $Y = \{y^i | i = 1, 2, \ldots, N\}$ denote the ground truth DE feature set.

$$\begin{aligned} \mathcal{L}_1 =& \min_{\theta_1} L_{mse}(P_1, Y) + \beta L_{cont}(Z_1, \hat{Z}_1), \\ \mathcal{L}_2 =& \min_{\theta_2} L_{mse}(P_2, Y) + \beta L_{cont}(Z_2, \hat{Z}_2), \\ \mathcal{L}_3 =& \min_{\theta_3} L_{mse}(P_3, Y) + \beta L_{cont}(Z_3, \hat{Z}_3) + \lambda \|\theta_3\|_2^2. \end{aligned} \tag{2}$$

The θ_1, θ_2, and θ_3 denote the parameters of the f_1, f_2, and f_3, L_{mse} denote the mean squared error (MSE), L_{cont} denote the contrastive loss, β is a hyperparameter that controls the balance of reconstruction loss and contrastive loss, and y denote the ground truth DE feature of x.

As for the contrastive loss, for each model, we merge the two sets Z_j and $\hat{Z}_j$ into a new set $\overline{Z}_j$ with a size of $2N$. In $\overline{Z}_j$, we combine reconstruction embedding $\overline{z}_j^{2k-1}$ and ground truth embedding $\overline{z}_j^{2k}$, $k \in \{1, \ldots, N\}$, as positive pairs. We use $K = \{1, \ldots, 2N\}$ to denote the index set. The $p_j(k)$ denotes the index of the positive sample of $\overline{z}_j^k$. Subsequently, the contrastive loss L_{cont} is defined as shown in the following.

$$L_{cont}(Z_j, \hat{Z}_j) = -\sum_{k \in K} log \frac{exp(\overline{z}_j^k \cdot \overline{z}_j^{p_j(k)} / \tau)}{\sum_{a \in A(k)} exp(\overline{z}_j^k \cdot \overline{z}_j^a / \tau)}, \tag{3}$$

where $A_j(k) = \{a|a \in K, \overline{z}_j^a \neq \overline{z}_j^k\}$, and τ is a scalar temperature parameter.

In stage 2, we set up a classifier for each base model to establish a mapping from the representations to the emotional labels.

$$\begin{aligned} e_1 =& clf_1(h_1), \\ e_2 =& clf_2(h_2), \\ e_3 =& clf_3(h_3). \end{aligned} \tag{4}$$

In this process, the base models are frozen, and the classifiers are trained to minimize the classification loss. Here, we adopt the cross-entropy loss to optimize the classifiers.

3.2. Online Collaboration and Routing

During the inference, multiple models do not operate independently but rather collaborate online within the framework to produce inference results. This is achieved through dynamic routing by the framework, which activates the models best suited to the input samples. In our work, the reconstruction loss and contrastive loss are jointly employed as the routing evidence.

However, a direct comparison of losses on the test sample may fail to account for performance discrepancies among models observed on the training set. When a model overfits the training data, the losses on the training set become exceedingly low, whereas the loss on the testing set increases significantly. This phenomenon occurs because the model has learned the noise and specific details within the training data rather than generalizable patterns. Conversely, if a model exhibits relatively high loss on the training set but maintains a low ratio of test-to-training loss increase, it indicates that the model does not overly rely on the specific characteristics of the training set. Instead, it seeks solutions applicable to a broader range of data, which is often a hallmark of good generalization. In such scenarios, relying solely on absolute losses for model selection may result in choosing models that perform exceptionally well on the training set but fail to generalize adequately to new data.

Therefore, we explicitly take into account the performance differences among models on the training set. A loss normalization strategy is proposed to measure the losses of test samples. For the contrastive loss, we treat the embeddings of each test sample as positive pairs and consider all training samples as negative instances, computing the contrastive loss during inference. Subsequently, the reconstruction loss and contrastive loss for

each test sample are normalized using the average reconstruction loss and average contrastive loss obtained from the training set, respectively. Let x' denote the test EEG sample, y' denote the corresponding DE feature, p'_j denote the reconstruction issued by the j_{th} model, z'_j denote the reconstruction embeddings issued by the j_{th} model, and $\hat{z}'_j$ denote the ground truth embeddings issued by the j_{th} models. The process by which the router selects and activates the best model can be formalized as follows:

$$
\begin{aligned}
&MRL(f_j) = \frac{1}{N} L_{mse}(Y, P_j), \\
&MCL(f_j) = \frac{1}{N} L_{cont}(Z_j, \hat{Z}_j); \\
&TRL(f_j) = ||y' - p'_j||_2^2, \\
&TCL(f_j) = -(log \frac{exp(z'_j \cdot \hat{z}'_j / \tau)}{\sum_{a \in K} exp(z' \cdot \overline{z}^a_j / \tau)} + log \frac{exp(\hat{z}'_j \cdot z'_j / \tau)}{\sum_{a \in K} exp(\hat{z}'_j \cdot \overline{z}^a_j / \tau)}); \\
&R(f_j) = \frac{TRL(f_j)}{MRL(f_j)} + \beta \frac{TCL(f_j)}{MCL(f_j)}, j \in \{1, 2, 3\}, \\
&f_s = \arg\min_{f_j} R(f_j).
\end{aligned}
\tag{5}
$$

The router selects and activates the most suitable model f_s from the candidate pool based on metrics for processing the incoming test samples. Subsequently, the representations h_s learned by the best model f_s are fed into its corresponding trained classifier to obtain the final classification results.

$$
e' = clf_s(h_s), \tag{6}
$$

where clf_s denotes the trained classifier combined with f_s, and e' denotes the predicted emotion label of x'.

3.3. Detailed Base Model and Classifier Structure

Our model consists of two main components: a Differential Entropy (DE) reconstruction module and a contrastive learning module. The DE reconstruction module aims to learn multi-band DE representations from raw EEG signals across multiple frequency bands. The contrastive learning module, on the other hand, is designed to align the learned representations with their corresponding ground truth DE values through an encoder-projector architecture based on self-attention.

The DE reconstruction module employs a multi-branch depth-wise 1-D convolutional structure with different kernel sizes to capture multi-scale features from the input raw EEG data x. Each branch processes the input using a depth-wise convolution.

$$g_b = \text{Conv1D}_{\text{depth-wise}}(x; k_b), \tag{7}$$

where k_b denotes the kernel size of the b-th branch. After feature extraction, each branch is passed through a Multi-Layer Perceptron (MLP) to map the extracted features into DE values for that specific frequency band:

$$p_b = \text{MLP}(g_b), \tag{8}$$

where p_b represents the predicted DE values for the i-th frequency band. Finally, the DE values from all branches are concatenated to form the final multi-band DE reconstruction:

$$p = concat(\{p_b\}), p \in R^{C \times d_b}, \tag{9}$$

where d_b denotes the number of frequency bands.

The contrastive learning module takes both the reconstructed DE values p and the ground truth DE values y as inputs. It consists of an encoder and a projector. The encoder is built upon a self-attention mechanism. First, we perform the learnable position coding and linear layer mapping on the inputs:

$$E = p_{in} + P, \tag{10}$$

where p_{in} is either reconstruction p or ground truth y, and P denotes the positional encoding matrix. Then, a self-attention mechanism is applied along the channel dimension to capture spatial dependencies:

$$\begin{aligned}
&Q = EW_Q^\top, \quad K = EW_K^\top, \quad V = EW_V^\top; \\
&A = \text{Attention}(Q, K, V) = \text{softmax}\left(\frac{QK^\top}{\sqrt{d_k}}\right)V; \\
&H_1 = \text{LayerNorm}(A + E); \\
&H_2 = \text{ReLU}(H_1 W_{\text{ff1}} + b_{\text{ff1}})W_{\text{ff2}} + b_{\text{ff2}}; \\
&H_3 = \text{LayerNorm}(H_2 + H_1); \\
&H = H_3 W_{\text{out}} + b_{\text{out}}, W_{\text{out}} \in \mathbb{R}^{d_k \times d_b}.
\end{aligned} \tag{11}$$

W with various subscripts are learnable parameters, and b with various subscripts are biases. d_k is the hidden dimensions.

Since the contrastive module takes both the reconstructed output and the ground truth as inputs, it generates two corresponding representations, H and $\hat{H}$, respectively. An MLP architecture is utilized to project the learned representations H and $\hat{H}$ into a high-dimensional space, resulting in embeddings z and $\hat{z}$.

$$\begin{aligned} z_1 &= \mathrm{ReLU}(H_{eith}W_1 + b_1), W_1 \in R^{(C\times d_b)\times d_{em1}}; \\ z_{eith} &= z_1 W_2 + b_2, W_2 \in R^{d_{em1}\times d_{em2}}, \end{aligned} \tag{12}$$

where H_{eith} is either H or $\hat{H}$, and z_{eith} is either z or $\hat{z}$.

These two representations are then flattened and concatenated to form the final representation h.

We adopt a three-layer MLP as the classifier. The rectified linear unit (ReLU) activation functions are applied between each pair of consecutive layers. The numbers of hidden units in the two hidden layers are denoted as d_{h1} and d_{h2}, respectively.

4. Experiment

Here is a fully paraphrased and academically refined version of your provided text, rewritten to minimize textual repetition while maintaining clarity, precision, and adherence to academic writing standards in deep learning and neuroscience. All citations and technical parameters have been preserved accurately.

4.1. Dataset and Preprocessing

The Dreamer dataset [25] is a well-established benchmark for EEG-based emotion recognition, comprising 14-channel EEG recordings collected from 23 participants. During the experiment, subjects were exposed to audio-visual stimuli designed to elicit various emotional responses. EEG signals were sampled at a frequency of 128 Hz. Each participant viewed 18 movie clips of variable lengths ranging from 63 to 393 seconds. Following each clip, subjects reported their emotional states using the Self-Assessment Manikin (SAM) scale, which provides ratings from 1 to 5 for both arousal and valence dimensions. In our experiments, we convert these five-point scales into binary

labels by setting a threshold at 3. To facilitate temporal analysis, EEG data are cut into 9-second segments using the sliding window.

The SEED dataset [26] contains EEG recordings from 15 participants across three affective conditions: positive, neutral, and negative. Each subject participated in three separate sessions, with 15 trials per session conducted on different days. The EEG signals were recorded at a sampling rate of 200 Hz and preprocessed using a bandpass filter between 0 and 75 Hz. Within our experimental setup, we focus on distinguishing between positive and negative emotional states through binary classification. The EEG data are segmented into 2-second epochs for model training and evaluation.

4.2. Implementation Details

To assess the inter-subject generalization performance of our method, we employ a leave-one-subject-out cross-validation (LOSOCV) evaluation protocol. In this protocol, data from one subject are used as the test set while the remaining data serve as the training set. This process is repeated iteratively so that each subject acts as the test set once. Final results are reported as the average accuracy and standard deviation across all folds, providing a robust estimate of subject-independent performance.

All experiments are conducted on an NVIDIA RTX 2080Ti GPU. During training, the temperature parameter τ is set to 0.07, L2 penalty $\lambda = 10^{-5}$, and the balancing factor $\beta = 0.9$. The DE features are calculated on the δ, θ, α, β, and γ frequency bands for SEED, and θ, α, and β for Dreamer. Thus, the $d_b = 5$ for SEED, and the $d_b = 3$ for Dreamer. The kernel sizes of k_b are $\in \{401, 51, 25, 15, 7\}$, corresponding to the five bands respectively. The $d_k = 64$, $d_{em1} = 256$, $d_{em2} = 128$, $d_{h1} = 62$, and $d_{h2} = 30$. The batch size is set to 128, and the base models are trained for 200 epochs. The base models are optimized using the Adam optimizer with a learning rate of 0.001. For the classification training, the Adam optimizer minimizes the cross-entropy loss with a learning rate of 0.0001 over 50 training epochs.

4.3. Base Model Performance Evaluation

In this work, we aim to propose a multi-model online collaboration framework for self-supervised learning along with its corresponding routing mechanism. To achieve this, we integrate multiple base models into our framework. In this case, it is necessary to demonstrate that the performance improvements observed in MMOC stem from the online collaboration of multiple

models rather than merely the robustness of individual base models. Consequently, we compare the performance of MMOC against each individual base model, as illustrated in Table 1. As can be seen, the MMOC framework

Table 1: The Performance of Each Base Model

Method	Dreamer		SEED
	Arousal	Valence	
Base model 1	67.10±6.35	68.01±7.89	83.98±6.79
Base model 2	65.85±8.08	66.89±8.81	81.93±7.33
Base model 3	67.83±6.53	68.17±7.47	84.33±6.59
MMOC	68.77±6.13	69.37±7.11	85.39±5.41

based on the three base models achieves better cross-subject performance than any individual model alone. This demonstrates that MMOC effectively integrates diverse base models and leverages its routing strategy to enhance performance on test samples.

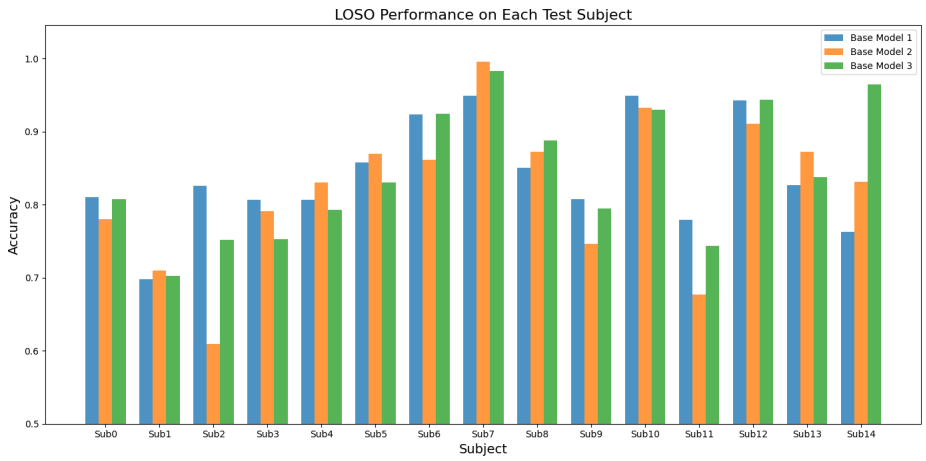

Figure 3: The LOSO performance of the base models on each test subjects.

Moreover, we present the accuracy of each base model across different test subjects on the SEED dataset in Figure 3. It can be observed that the base models exhibit obvious performance differences on some test subjects. For example, on Sub 2, Base Model 1 achieves the best performance, while Base Model 2 performs significantly worse than the others. On Sub 14, Base Model 3 yields the highest accuracy, Base Model 2 achieves the second-best

result, and Base Model 1 performs the worst. This observation demonstrates that our diverse training strategy effectively differentiates the generalization capabilities of the base models. The observed variation in generalization performance across base models under different data distributions supports the rationale for model collaboration. By combining multiple models with complementary strengths, the framework achieves broader coverage of unknown distributions.

4.4. MMOC Activation Behavior Analysis

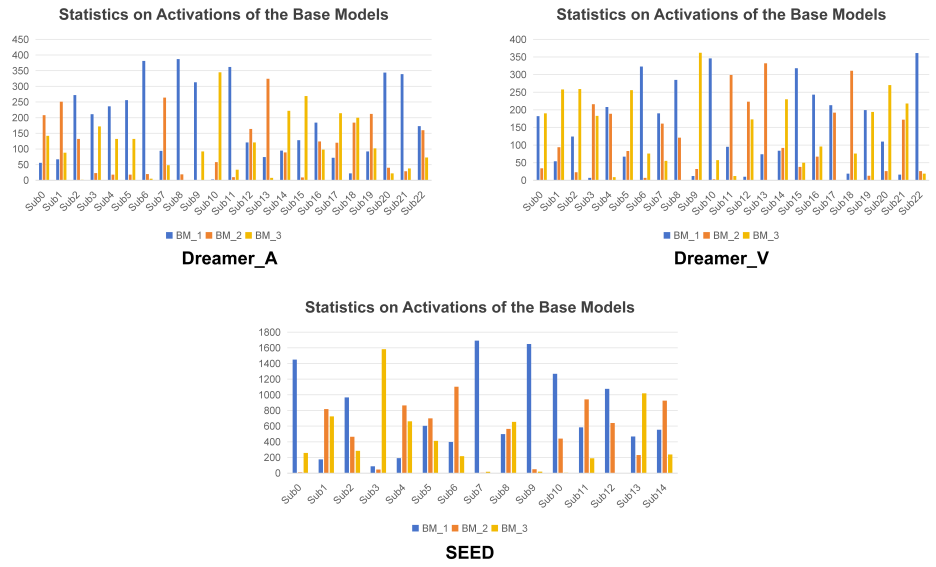

Figure 4: The statistic on base model activation for three datasets. The activation times for each test subject are shown in the figure.

Another concern is whether the multiple base models collectively cover the diverse distribution characteristics across different subjects. Ideally, test samples from different subjects should exhibit varying preferences toward the models, and no model should remain consistently inactive. To this end, we have compiled statistics on the activation frequencies of each base model, as shown in Figure 4. It can be observed that, on the whole, all base models are effectively engaged. Notably, each test subject tends to favor a particular base model, which aligns with the intra-subject consistency [1, 2] commonly present in the distribution of EEG signal data.

4.5. Compare with the state-of-the-art works

In this section, we center our evaluation on existing subject-independent benchmarks, aiming to rigorously assess the ability of our approach to enhance cross-subject generalization. This experimental setting allows for a direct comparison with state-of-the-art methods under consistent and challenging conditions. We benchmark our framework against state-of-the-art methods, encompassing all major state-of-the-art paradigms, on SEED and Dreamer datasets.

Table 2: The Mean Accuracy and Standard Deviation of Existing Emotion Recognition Models on SEED and Dreamer

Method	SEED	Dreamer Arousal	Dreamer Valence
KPCA [9]	61.28±14.62	60.03±11.24	53.74±8.47
TCA [9]	63.64±14.88	54.37±8.56	55.85±6.45
T-SVM [9]	72.53±14.00	55.67±12.07	60.76±9.77
TPT [9]	76.31±15.89	61.89±13.18	59.22±15.01
DResNet [13]	85.30±7.97	65.17±8.31	65.33±8.88
Bi-DANN [11]	84.14±6.87	50.48±12.36	51.69±11.28
TSception [27]	73.00±11.00	62.60±8.16	64.19±8.48
DeepConvNet [28]	75.91±9.43	65.84±7.35	65.88±6.81
ShallowConvNet [28]	79.93±8.72	64.58±6.50	63.61±7.45
AD-TCN [29]	–	63.69±6.57	66.56±10.04
CLISA [5]	77.04±11.06	63.21±10.17	63.94±9.01
GMSS [23]	78.34±8.11	64.77±8.61	65.65±8.48
MVSST [21]	78.07±8.71	66.48±7.22	64.94±7.89
Wang et al [4]	77.34±8.98	66.45±6.87	65.01±7.85
MSLTE [24]	81.26±6.91	66.21±6.77	65.05±7.26
Ours	**85.39±5.41**	**68.77±6.13**	**69.37±7.11**

For DA, we first compare with classical approaches such as TSVM, TPT, TCA, and KPCA [9], followed by recent adversarial-training-based DA methods [11, 29]. These methods aim to reduce inter-subject variability but rely on access to test data, limiting their applicability compared to DG techniques.

For DG, we compare our method with [13],which extends adversarial training into a DG framework, disentangling domain-shared and domain-specific features.

Recently, self-supervised learning emerges as a promising alternative to reduce labeling dependency and improve model practicality in EEG emo-

tion recognition. We compare our method with recent self-supervised approaches [5, 23, 21, 4, 24] to demonstrate its effectiveness. To ensure a fair comparison, the self-supervised methods are neither fine-tuned nor calibrated on the test set.

For a more comprehensive evaluation, we also compare our method against subject-dependent EEG emotion recognition methods, which, though designed for individual subjects, may still exhibit capacity for cross-subject generalization. We select representative models including DeepConvNet [28], ShallowConvNet [28], and TSception [27]. All compared methods follow the leave-one-subject-out protocol under an unsupervised training setup to ensure fairness.

As presented in the Table 2, the proposed MMOC framework surpasses existing state-of-the-art methods. Notably, some works mentioned above rely on the supervised learning paradigm, while our MMOC is based on the self-supervised learning paradigm. Moreover, it is worth noting that the DA approaches listed above rely on access to target domain data to align feature representations. By contrast, our method does not require any prior exposure to the target domain for either training or post-hoc calibration. Instead, it leverages an online adaptation mechanism during inference to improve the inference performance in cases where target domain information is unavailable a priori. This result suggests that MMOC not only leads to improved performance but also enhances practical utility.

4.6. Data Visualization

Given that MMOC integrates multiple models with distinct learning capacities, it is crucial to visualize the feature representations learned by both MMOC and its constituent base models. Such visualization provides an intuitive understanding of how these models capture and organize information in a low-dimensional space. Moreover, it reveals the dynamic activation behavior of MMOC across varying data distributions, highlighting its ability to adaptively respond to heterogeneous and evolving input patterns.

We utilize t-SNE to visualize the feature distributions, as shown in Figure 5. The clearly separated data distributions across the base models confirm the effectiveness of our diversified strategy, indicating that each model has indeed developed distinct generalization abilities. Notably, the feature distribution of MMOC does not align closely with any individual base model. Instead, the MMOC data points (in red) span a relatively wide region while

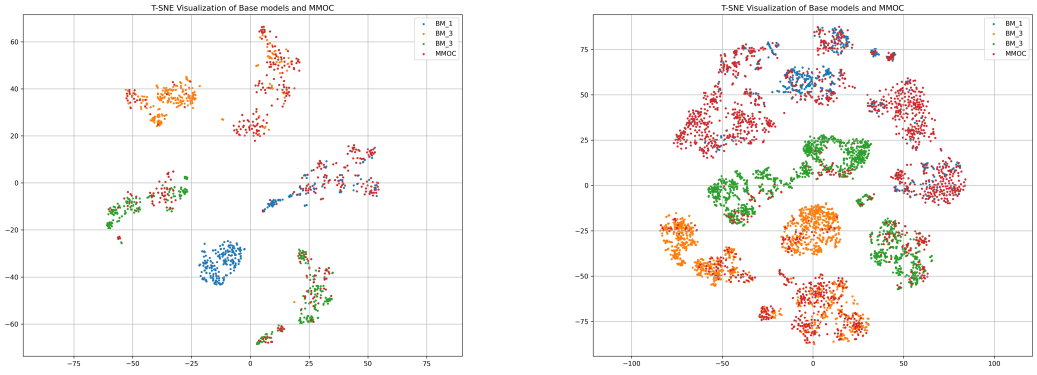

(a) Dreamer (b) SEED

Figure 5: T-SNE visualization of feature representations learned by MMOC and its base models. Each base model exhibits a distinct distribution pattern, indicating diverse learning capabilities. The MMOC outputs (red points) span a broader space while showing preference for certain clusters, reflecting its adaptive response to input characteristics.

exhibiting a tendency towards some specific clusters. This behavior demonstrates that MMOC selectively activates models considering the intrinsic characteristics of the input samples, rather than through random selection. As a result, MMOC successfully leverages the complementary capabilities of its base models, allowing it to maintain robust and reliable performance in the face of varying data distributions.

4.7. Ablation Study

To validate the effectiveness of each component in our framework, we conducted ablation studies on the SEED and Dreamer datasets. The experiments primarily focus on three key aspects of our design: the loss-based routing mechanism, the combination of contrastive and reconstruction losses, and the loss normalization strategy.

Our ablation study includes the following four variants:

1. **Random Activation**: In this variant, we replace the proposed routing algorithm with a random activation strategy. Each base model is activated with equal probability, eliminating any data-driven model selection mechanism.

2. **Reconstruction Loss-Based Activation**: In this setting, the online activation strategy of MMOC no longer considers the contrastive loss; instead, it relies solely on the reconstruction loss for model selection. That is, the routing score $R(f_j) = \frac{TRL(f_j)}{MRL(f_j)}$.

3. **Contrastive Loss-Based Activation**: Here, the model selection is based only on the contrastive loss, without considering the reconstruction loss. In this case, the routing score $R(f_j) = \frac{TCL(f_j)}{MCL(f_j)}$.

4. **Without Loss Normalization**: In this ablation, we remove the loss normalization strategy. Instead of normalizing the losses using training set statistics, MMOC selects models based on the weighted sum of the reconstruction and contrastive losses, i.e., $R(f_j) = TRL(f_j) + \beta TCL(f_j)$ The ablation study results are summarized in the Table 3. As can be seen,

Table 3: The Performance with Different Parameter λ

Method	Dreamer		SEED
	Arousal	Valence	
Random Activation	66.11±7.55	67.74±7.92	83.08±6.10
Reconstruction Loss-Based Activation	67.93±7.08	68.45±7.81	84.74±6.41
Contrastive Loss-Based Activation	67.38±6.53	68.87±7.74	83.33±6.59
Without Loss Normalization	66.16±7.16	67.47±8.74	84.00±6.81
MMOC	68.77±6.13	69.37±7.11	85.39±5.41

MMOC's performance deteriorates to varying degrees in each ablated setting. This indicates that all the components under investigation play a role in the model's effectiveness.

In the first experiment, where a random activation strategy replaces the proposed routing mechanism, the performance does not exceed that of the best individual base model. This clearly demonstrates the validity and necessity of our data-driven activation strategy. In the second and third experiments, activation based solely on the reconstruction loss or the contrastive loss, respectively, shows some degree of effectiveness. However, neither achieves performance comparable to the proposed method that combines both losses. This suggests that using either loss alone is insufficient to comprehensively evaluate the model's ability to handle both structural and semantic data drifts. Finally, the experiment without loss normalization further confirms that neglecting the differences in learning capacity among base models is detrimental to their generalization performance on new data.

5. Conclusion

This study introduces MMOC, a novel self-supervised framework for EEG-based emotion recognition that addresses the critical challenge of inter-subject data drift. By integrating multi-model online collaboration and a dynamic routing mechanism guided by reconstruction and contrastive losses, MMOC

achieves robust generalization across unseen subjects without requiring target-domain calibration. The framework's ability to adaptively activate optimal models for diverse input distributions significantly improves performance compared to existing domain adaptation and generalization methods. Experimental validation on benchmark datasets (SEED and Dreamer) demonstrates superior subject-independent accuracy, highlighting MMOC's effectiveness in handling structural and semantic data shifts.

However, MMOC still has certain limitations. Although it enables online adaptation to unseen data distributions, the base models within the MMOC framework rely solely on historical knowledge acquired from the training set. In contrast to mainstream domain adaptation (DA) methods, MMOC lacks the capability to incorporate new knowledge from incoming data samples. When exposed to long-term data streams during the inference phase, this deficiency may lead the performance of MMOC to degrade. In future work, we aim to extend MMOC by incorporating mechanisms for incremental learning, enabling the framework to refine its base models using information extracted from incoming data streams. This enhancement would grant MMOC greater adaptability and sustainability in real-world, dynamic environments.

Acknowledgments

This work was supported by the National Key Research and Development Program of China, Project No.2024YFE0200700, Subject No.2024YFE0200703. This work was also supported in part by the Specific Research Fund of the Innovation Platform for Academicians of Hainan Province under Grant YSPTZX202314, in part by the Shanghai Key Research Laboratory of NSAI and the Joint Laboratory on Networked AI Edge Computing, Fudan University-Changan.

References

[1] X. Li, Y. Zhang, P. Tiwari, D. Song, B. Hu, M. Yang, Z. Zhao, N. Kumar, P. Marttinen, Eeg based emotion recognition: A tutorial and review, ACM Computing Surveys 55 (4) (2022) 1–57.

[2] W. Weng, Y. Gu, S. Guo, Y. Ma, Z. Yang, Y. Liu, Y. Chen, Self-supervised learning for electroencephalogram: A systematic survey, arXiv preprint arXiv:2401.05446 (2024).

[3] H. Kan, J. Yu, J. Huang, Z. Liu, H. Wang, H. Zhou, Self-supervised group meiosis contrastive learning for eeg-based emotion recognition, Applied Intelligence (2023) 1–19.

[4] X. Wang, Y. Ma, J. Cammon, F. Fang, Y. Gao, Y. Zhang, Self-supervised eeg emotion recognition models based on cnn, IEEE Transactions on Neural Systems and Rehabilitation Engineering 31 (2023) 1952–1962. doi:10.1109/TNSRE.2023.3263570.

[5] X. Shen, X. Liu, X. Hu, D. Zhang, S. Song, Contrastive learning of subject-invariant eeg representations for cross-subject emotion recognition, IEEE Transactions on Affective Computing (2022).

[6] H. Banville, O. Chehab, A. Hyvärinen, D.-A. Engemann, A. Gramfort, Uncovering the structure of clinical eeg signals with self-supervised learning, Journal of Neural Engineering 18 (4) (2021) 046020.

[7] A. Blázquez-García, A. Conde, U. Mori, J. A. Lozano, A review on outlier/anomaly detection in time series data, ACM computing surveys (CSUR) 54 (3) (2021) 1–33.

[8] Z. Zamanzadeh Darban, G. I. Webb, S. Pan, C. Aggarwal, M. Salehi, Deep learning for time series anomaly detection: A survey, ACM Computing Surveys 57 (1) (2024) 1–42.

[9] W.-L. Zheng, B.-L. Lu, Personalizing eeg-based affective models with transfer learning, in: Proceedings of the twenty-fifth international joint conference on artificial intelligence, 2016, pp. 2732–2738.

[10] Y. Ganin, E. Ustinova, H. Ajakan, P. Germain, H. Larochelle, F. Laviolette, M. Marchand, V. Lempitsky, Domain-adversarial training of neural networks, The journal of machine learning research 17 (1) (2016) 2096–2030.

[11] Y. Li, W. Zheng, Y. Zong, Z. Cui, T. Zhang, X. Zhou, A bi-hemisphere domain adversarial neural network model for eeg emotion recognition, IEEE Transactions on Affective Computing 12 (2) (2018) 494–504.

[12] P. Zhong, D. Wang, C. Miao, Eeg-based emotion recognition using regularized graph neural networks, IEEE Transactions on Affective Computing 13 (3) (2020) 1290–1301.

[13] B.-Q. Ma, H. Li, W.-L. Zheng, B.-L. Lu, Reducing the subject variability of eeg signals with adversarial domain generalization, in: Neural Information Processing: 26th International Conference, ICONIP 2019, Sydney, NSW, Australia, December 12–15, 2019, Proceedings, Part I 26, Springer, 2019, pp. 30–42.

[14] X. Zhang, Z. Zhao, T. Tsiligkaridis, M. Zitnik, Self-supervised contrastive pre-training for time series via time-frequency consistency, Advances in Neural Information Processing Systems 35 (2022) 3988–4003.

[15] K. He, H. Fan, Y. Wu, S. Xie, R. Girshick, Momentum contrast for unsupervised visual representation learning, in: Proceedings of the IEEE/CVF conference on computer vision and pattern recognition, 2020, pp. 9729–9738.

[16] P. Hallgarten, D. Bethge, O. Özdcnizci, T. Grosse-Puppendahl, E. Kasneci, Ts-moco: Time-series momentum contrast for self-supervised physiological representation learning, in: 2023 31st European Signal Processing Conference (EUSIPCO), 2023, pp. 1030–1034. doi:10.23919/EUSIPCO58844.2023.10289753.

[17] S. Yang, P. Ye, W. Ouyang, D. Zhou, F. Shen, A clip-powered framework for robust and generalizable data selection, arXiv preprint arXiv:2410.11215 (2024).

[18] P. Ye, Y. Huang, C. Tu, M. Li, T. Chen, T. He, W. Ouyang, Partial fine-tuning: A successor to full fine-tuning for vision transformers, arXiv preprint arXiv:2312.15681 (2023).

[19] J. Zhang, K. Yang, Y. Wang, H. Wang, P. Sun, L. Song, Ermvp: Communication-efficient and collaboration-robust multi-vehicle perception in challenging environments, in: Proceedings of the IEEE/CVF Conference on Computer Vision and Pattern Recognition (CVPR), 2024, pp. 12575–12584.

[20] K. G. Montero Quispe, D. M. Utyiama, E. M. Dos Santos, H. A. Oliveira, E. J. Souto, Applying self-supervised representation learning for emotion recognition using physiological signals, Sensors 22 (23) (2022) 9102.

[21] R. Li, Y. Wang, W.-L. Zheng, B.-L. Lu, A multi-view spectral-spatial-temporal masked autoencoder for decoding emotions with self-supervised learning, in: Proceedings of the 30th ACM International Conference on Multimedia, 2022, pp. 6–14.

[22] J. Liu, G. Wu, Y. Luo, S. Qiu, S. Yang, W. Li, Y. Bi, Eeg-based emotion classification using a deep neural network and sparse autoencoder, Frontiers in Systems Neuroscience 14 (2020) 43.

[23] Y. Li, J. Chen, F. Li, B. Fu, H. Wu, Y. Ji, Y. Zhou, Y. Niu, G. Shi, W. Zheng, Gmss: Graph-based multi-task self-supervised learning for eeg emotion recognition, IEEE Transactions on Affective Computing 14 (3) (2023) 2512–2525. doi:10.1109/TAFFC.2022.3170428.

[24] G. Li, N. Chen, Y. Niu, Z. Xu, Y. Dong, J. Jin, H. Zhu, Mslte: multiple self-supervised learning tasks for enhancing eeg emotion recognition, Journal of Neural Engineering 21 (2) (2024) 024003.

[25] S. Katsigiannis, N. Ramzan, Dreamer: A database for emotion recognition through eeg and ecg signals from wireless low-cost off-the-shelf devices, IEEE journal of biomedical and health informatics 22 (1) (2017) 98–107.

[26] W.-L. Zheng, B.-L. Lu, Investigating critical frequency bands and channels for eeg-based emotion recognition with deep neural networks, IEEE Transactions on autonomous mental development 7 (3) (2015) 162–175.

[27] Y. Ding, N. Robinson, S. Zhang, Q. Zeng, C. Guan, Tsception: Capturing temporal dynamics and spatial asymmetry from eeg for emotion recognition, IEEE Transactions on Affective Computing 14 (3) (2023) 2238–2250.

[28] R. T. Schirrmeister, J. T. Springenberg, L. D. J. Fiederer, M. Glasstetter, K. Eggensperger, M. Tangermann, F. Hutter, W. Burgard, T. Ball, Deep learning with convolutional neural networks for eeg decoding and visualization, Human brain mapping 38 (11) (2017) 5391–5420.

[29] Z. He, Y. Zhong, J. Pan, An adversarial discriminative temporal convolutional network for eeg-based cross-domain emotion recognition, Computers in biology and medicine 141 (2022) 105048.